# Hydrogen Bonding Networks Tune Proton-Coupled Redox Steps during the Enzymatic Six-Electron Conversion of Nitrite to Ammonia

Evan T. Judd,[†] Natalia Stein,[‡] A. Andrew Pacheco,[‡] and Sean J. Elliott*,[†]

[†]Department of Chemistry, Boston University, 590 Commonwealth Avenue, Boston, Massachusetts 02215, United States
[‡]Department of Chemistry and Biochemistry, University of Wisconsin—Milwaukee, Milwaukee, Wisconsin 53211, United States

**S** *Supporting Information*

**ABSTRACT:** Multielectron multiproton reactions play an important role in both biological systems and chemical reactions involved in energy storage and manipulation. A key strategy employed by nature in achieving such complex chemistry is the use of proton-coupled redox steps. Cytochrome *c* nitrite reductase (ccNiR) catalyzes the six-electron seven-proton reduction of nitrite to ammonia. While a catalytic mechanism for ccNiR has been proposed on the basis of studies combining computation and crystallography, there have been few studies directly addressing the nature of the proton-coupled events that are predicted to occur along the nitrite reduction pathway. Here we use protein film voltammetry to directly interrogate the proton-coupled steps that occur during nitrite reduction by ccNiR. We find that conversion of nitrite to ammonia by ccNiR adsorbed to graphite electrodes is defined by two distinct phases; one is proton-coupled, and the other is not. Mutation of key active site residues (H257, R103, and Y206) modulates these phases and specifically alters the properties of the detected proton-dependent step but does not inhibit the ability of ccNiR to conduct the full reduction of nitrite to ammonia. We conclude that the active site residues examined are responsible for tuning the protonation steps that occur during catalysis, likely through an extensive hydrogen bonding network, but are not necessarily required for the reaction to proceed. These results provide important insight into how enzymes can specifically tune proton- and electron transfer steps to achieve high turnover numbers in a physiological pH range.
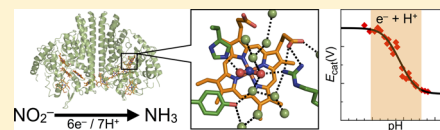
Multielectron multiproton reactions are at the core of many chemical reactions important in biology,[1] as well as nearly every reaction important in energy conversion.[2] These reactions present a number of challenges, including the achievement of the complete reaction of substrate without the release of reactive intermediates, avoiding the requirement of physiologically inaccessible reduction potentials, and ensuring the reaction proceeds across a relatively narrow window of potential.

One strategy employed by Nature to overcome the challenges inherent to multielectron multiproton chemistry is the use of proton-coupled electron transfer (PCET).[2−5] The coupled transfer of a proton and an electron is encountered in many biological systems, and these PCET processes have been well studied over the past several decades.[3,6] Many of these studies have focused on the role of PCET in transferring radical intermediates long-range,[7−9] in water oxidation,[10−12] and in the generation of proton gradients.[3,13,14] Studies focused on how PCET processes are governed during the transfer of multiple electrons and protons to a single substrate by an enzyme during catalysis are therefore of considerable importance for the development of a better understanding of these complex biological processes.

Cytochrome *c* nitrite reductase (ccNiR) is a periplasmic enzyme involved in bacterial respiratory nitrate ammonification. The ccNiR enzyme catalyzes the remarkable six-electron seven-proton reduction of nitrite to ammonia, the second step in the conversion of nitrate to ammonia.[15,16] The enzyme has also been shown to perform the two-electron reduction of

hydroxylamine and the five-electron reduction of nitric oxide.[17,18] Its ability to conduct such complex reactions at relatively high turnover numbers without the release of intermediates makes it a particularly interesting model for multielectron multiproton reactions.

The *Shewanella oneidensis* ccNiR enzyme is a homodimer, containing five *c*-type hemes per protomer.[19] Four of these hemes are bis-His-ligated and are presumably involved in the transfer of electrons to the active site heme, which is ligated by a single lysine residue and contains an open coordination site for substrate binding. The ccNiR hemes have been assigned potentials of −295, −230, −166, −105, and −36 mV at pH 6 using PFV.[19] The −105 mV heme is likely the active site heme, on the basis of potential assignments to individual hemes using EPR in the *Escherichia coli* enzyme, where the second heme to be reduced is the active site heme.[19,20] The active site of ccNiR is populated by a set of strongly conserved amino acid residues (Tyr206, His257, and Arg103) that are presumably involved in catalysis (Figure 1).

While a catalytic cycle has been proposed[16,21−23] (Scheme 1), there have been few studies providing direct experimental evidence of the nature of the ET and proton-coupled steps occurring during the conversion of nitrite to ammonia. Recently, we have shown that the reaction is likely conducted in a series of one-electron transformations.[19,24] Still lacking are
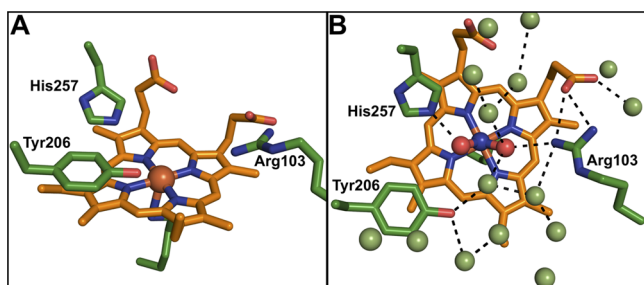
**Figure 1.** Architecture of the ccNiR active site. (A) Active site of *S. oneidensis* cytochrome *c* nitrite reductase.[19] (B) Active site of nitrite-bound *Wolinella succinogenes* ccNiR showing the hydrogen bonding network.[40] Key active site residues are colored green. Residues are numbered using *S. oneidensis* ccNiR numbering. Images generated in PyMol from Protein Data Bank entries 3UBR and 2E80, respectively.

**Scheme 1. Proposed Reaction Scheme for the Six-Electron Seven-Proton Reduction of Nitrite to Ammonia by ccNiR[a]**
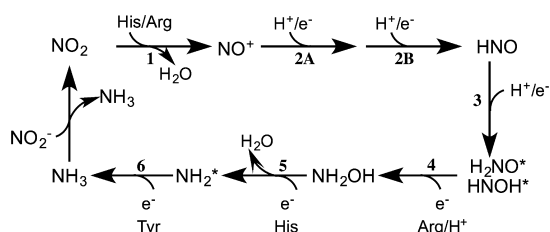


[a]Proposed radical intermediates are denoted with asterisks. Residues predicted to be involved in steps are denoted. Adapted from ref 25.

experimental data describing the nature of proton delivery steps occurring during catalysis in ccNiR. Computational studies using DFT have focused on PCET during ccNiR catalysis and offer a great deal of insight into the possible roles of the Tyr206, His257, and Arg103 active site amino acid residues.[21,22,25] To the best of our knowledge, there have been only limited studies probing the role of the active site residues in catalysis by ccNiR directly, a deficiency remedied by the work presented here.

Various ccNiR enzymes have been studied using protein film voltammetry (PFV),[24,26−28] revealing distinct electrochemical fingerprints characterized by attenuations ("switches") and enhancements ("boosts") in activity depending of the concentration of nitrite present. Here we seek to use PFV to improve our understanding of the mechanism by which ccNiR conducts the six-electron reduction of nitrite to ammonia, by coupling site-directed mutagenesis to variable-pH experiments, to directly probe the roles of individual active site residues in PCET processes.

Our findings expand our understanding of how coupling of protons to ET can be controlled within multielectron redox enzymes. We find that ccNiR nitrite electrocatalysis can be described as being governed by two components, a one-electron feature that is pH-independent and a one-electron feature that is coupled to a single protonation event, providing insight into the catalytic mechanism of this enzyme. Surprisingly, we also find that mutations of individual resides within the active site alter the nature of proton coupling but do not inhibit the ability of ccNiR to complete its reduction of nitrite to ammonia. This indicates that the rates and $pK_a$ values of proton-coupled steps are tightly governed by the residues within the active site, likely through an extensive hydrogen

bonding network, yet these residues do not necessarily direct the progression of the catalytic reduction of substrate to product.

## MATERIALS AND METHODS

**Enzyme Expression and Purification.** *S. oneidensis* TSP-C transformed with a TEV cleavable 10-histidine tag (C-terminal) in PHSG298[19] was grown in 1 L of 2×YT medium at 30 °C for 24 h. Cells were pelleted by centrifugation at 6000*g* for 12 min and resuspended in 20 mM 4-(2-Hydroxyethyl)piperazine-1-ethanesulfonic acid (HEPES) and 500 mM NaCl (pH 8) with 0.1 mM PMSF. Cells were lysed by sonication using 10 × 10 s bursts. The lysate was clarified by centrifugation at 18000*g* for 25 min. The clarified lysate was then loaded onto Ni-6-Sepharose resin (GE Healthcare) equilibrated with 20 mM HEPES, 500 mM NaCl, and 20 mM imidazole (pH 8). Bound protein was eluted with 20 mM HEPES, 500 mM NaCl, and 300 mM imidazole.

The His tag was then removed by digestion overnight with recombinant TEV protease in 50 mM HEPES, 500 mM NaCl, 1 mM DTT, and 0.5 mM EDTA (pH 8). The digested enzyme sample was then dialyzed into 20 mM HEPES, 500 mM NaCl, and 20 mM imidazole (pH 8). The sample was then loaded onto Ni-6-Sepharose resin, and the tagless flow-through was collected. Cleavage of the tag was usually >80% efficient. The enzyme was then concentrated and buffer exchanged into 20 mM HEPES and 200 mM NaCl (pH 8); glycerol was added to a concentration of 10%, and samples were stored at −80 °C. These preparations typically yielded 1 mg/L cell culture and were >95% pure as judged by sodium dodecyl sulfate−polyacrylamide gel electrophoresis. Wild-type ccNiR used in pH dependence experiments was purified as described previously.[19]

**Construction of Site-Directed Mutants.** Active site variants were constructed using an Agilent QuikChange Lightning kit with DNA primers listed in Table 1 of the Supporting Information. All mutations were verified by sequencing.

**Protein Film Voltammetry.** Protein film voltammetry experiments were conducted as previously described.[19,24] Briefly, small volumes of ccNiR were deposited onto pyrolytic graphite edge electrodes; the electrode was rinsed and then immersed in the electrochemical cell solution that consisted of a mixed buffer system of 5 mM sodium acetate, 5 mM CAPS, 6 mM CHES, 5 mM MOPS, 5 mM MES, 4 mM TAPS, 100 mM NaCl, and 2 mM CaCl₂, which allowed buffering over a wide range of pH values. All PFV experiments were conducted in an MBraun Labmaster inert chamber to prevent the background contribution of oxygen reduction at the graphite electrode.

Steady-state kinetic analysis was performed on wild-type (WT), Y206F, R103K, and R103Q variants by recording cyclic voltammograms of ccNiR at different nitrite concentrations and measuring the current magnitude (i.e., catalytic rate) at −550 mV.

Variable-pH experiments were performed by changing the pH of a master solution of buffer using HCl or NaOH, taking small aliquots at a given pH, purging the buffer with argon, and then bringing the samples into the inert chamber. Once a ccNiR film had been generated, the pH of the cell solution was changed by simply replacing the existing buffer with buffer at the new pH value and adding the desired concentration of nitrite. After each experiment, the cell solution was saved and

the pH recorded again to ensure the pH of the cell solution did not change during the electrocatalysis experiment.

**H257Q Specific Activity Experiments.** The specific activity of H257Q ccNiR was measured by following the oxidation of reduced methyl viologen at 600 nm ($\varepsilon = 13700$ $M^{-1}$ $cm^{-1}$) in 20 mM HEPES and 100 mM NaCl (pH 7) at 20 °C. Reactions were conducted in anaerobic vials and purged with argon to remove oxygen. Reactions were initiated by addition of 1 mM sodium nitrite. All reported values were corrected for nonenzymatic background reoxidation of methyl viologen.

**Quantification of Reducing Equivalent Consumption and Ammonia Production.** The number of moles of methyl viologen consumed per mole of ammonia produced was determined using a two-part assay. Ammonia detection was performed according to a modified protocol described by Chaney and Marbach.[29,30] Reagent 1 contained 0.625 g of NaOH and 200 $\mu$L of sodium hypochlorite (commercial bleach, 5.84% available chlorine) in 25 mL of deionized water. Reagent 2 contained 1.25 g of phenol and 0.00625 g of sodium nitroferricyanide in 25 mL of deionized water.

Assays were conducted in 20 mM HEPES and 100 mM NaCl (pH 7) at room temperature. Gastight syringes were used for manipulation of all solutions. Enzyme and reduced methyl viologen (final concentration of 500 $\mu$M) were added to a stoppered cuvette containing buffer that had been purged with argon. The recording of the absorbance at 600 nm was begun, and a baseline was recorded for ~30 s. The reaction was initiated with 1 mM sodium nitrite, and $A_{600}$ was recorded until all methyl viologen had been oxidized ($A_{600} = 0$).

Next, 400 $\mu$L of the reacted solution was mixed with 400 $\mu$L each of ammonia detection reagents 1 and 2. The mixture was incubated at 37 °C for 15 min, and the absorbance was measured at 625 nm. The concentration of ammonia was then calculated using a standard curve prepared with ammonium chloride. Final values for the number of moles of methyl viologen consumed per mole of ammonia produced were corrected for background levels of ammonia in reagents (using oxidized methyl viologen) and background nonenzymatic reoxidation of methyl viologen.

## ■ RESULTS

**WT and Mutant ccNiR Kinetics.** To assess the importance of proton delivery upon catalysis, PFV was used to determine kinetic values for WT and mutant ccNiR by following the limiting current ($i_{lim}$) at −550 mV with increasing nitrite concentrations (Table 1). For the WT enzyme, steady-state kinetic data for nitrite turnover fit well to a substrate inhibition model as was determined previously in PFV studies using the *Shewanella* ccNiR purified from a high-yield expression system.[19,24] The physical basis of the apparent substrate inhibition is still not well understood but may reflect the presence of asymmetry between protomers within the ccNiR dimer.[24] For all other mutants, kinetic data fit best to a simple Michaelis–Menten model of enzyme kinetics, in which the appearance of substrate inhibition is lost.

Y206F ccNiR was approximately 17-fold less active than WT with a 3-fold smaller $K_M$. R103Q ccNiR was approximately 2-fold less active than WT ccNiR but had a 9-fold larger $K_M$. For this reason, the R103K variant was constructed to investigate the possibility that a lost charge-based stabilization was responsible for the increased $K_M$ in the R103Q variant. It was

**Table 1. Kinetic Values of WT and Mutant ccNiR**[a]

| | $K_M$ ($\mu$M) | $k_{cat}$ ($e^-$ $s^{-1}$) | $k_{cat}$ (% of WT) | $K_I$ (mM) | mol of MV/ mol of NH$_4^+$ |
|---|---|---|---|---|---|
| WT | 100 ± 15 | 150 ± 20 | 100 | 11 | 5.0 ± 1.0 |
| H257Q | ND[c] | ND[c] | 0.8[b] | ND[c] | 6.4 ± 0.6 |
| Y206F | 35 ± 15 | 9 ± 3 | 6.0 | NA[d] | 5.5 ± 0.1 |
| R103Q | 910 ± 130 | 82 ± 9 | 55 | NA[d] | 6.3 ± 0.5 |
| R103K | 340 ± 50 | 20 ± 5 | 13 | NA[d] | 6.0 ± 0.6 |

[a]All kinetic parameters were determined by PFV as described in Materials and Methods with the exception of H257Q. [b]Because of low activity, the H257Q percent activity was measured in solution at 1 mM nitrite, pH 7, and 20 °C and compared to that of WT ccNiR, also measured in solution, under the same conditions. PFV was conducted at pH 7 and 20 mV/s with a rotation rate of 3000 rpm. [c]Not determined. [d]Not available.

found that R103K ccNiR had a $K_M$ closer to that of WT, but with a lower activity.

The activity of H257Q was found to be too low to measure using PFV, so using a standard solution assay with 1 mM nitrite, the activity was found to be reduced by approximately 150-fold compared to the WT ccNiR activity measured in solution under the same conditions (Table 1). (Because of the very low activity, catalytic PFV could not be used to further characterize the H257Q variant.)

**WT Catalytic Current–Potential Profile.** As found previously, examining a range of nitrite concentrations that span the $K_M$ value, at pH 7, WT ccNiR displays the same evidence of a preliminary onset of catalysis (centered at $E_{cat1}$), a secondary depletion of activity ($E_{sw}$), and a secondary increase in activity (centered at $E_{cat2}$) as the concentration of nitrite becomes sufficiently high (Figure 2).[24] The potential of $E_{cat1}$ is dependent on the concentration of nitrite and varies from −200 to −250 mV across the range of concentrations of nitrite tested (Figure 2A, inset). The boost feature, $E_{cat2}$, appears at −365 mV at the highest concentration of nitrite under these conditions.

The relative contribution of both catalytic features to the overall waveform is dependent on pH (Figure 3). At pH 7 and 500 $\mu$M nitrite (greater than $K_M$), both features are present, but the $E_{cat2}$ feature is visible only as a low-potential shoulder at the highest nitrite concentrations. This feature becomes much more prominent at higher pH values, and at pH >8, the $E_{cat2}$ feature dominates waveforms produced at high nitrite concentrations. At lower pH values and high nitrite concentrations, the waveform is dominated by $E_{cat1}$, and $E_{cat2}$ is barely visible. At pH <5.5, no boost is observed at low nitrite concentrations.

**Y206F Catalytic Current–Potential Profile.** Mutation of Y206 to a phenylalanine drastically alters the catalytic current–potential profile during nitrite turnover (Figure 2B). Y206F ccNiR current–potential profiles are characterized by the presence of two catalytic features, which are easily resolved from one another across all nitrite concentrations at pH 7. No "switch" feature is observed under any of the conditions tested. At sub-$K_M$ nitrite concentrations, the catalytic wave is dominated by a single feature, $E_{cat1}$, which is nearly indistinguishable from the nonturnover signal caused by the low activity of this mutant. Only a very small boost in activity centered at $E_{cat2}$ is observed under these conditions. As the nitrite concentration is increased, $E_{cat2}$ begins to dominate the waveform. At saturating nitrite concentrations, $E_{cat1}$ is visible only as a high-potential shoulder in the first derivative of the catalytic waveform.
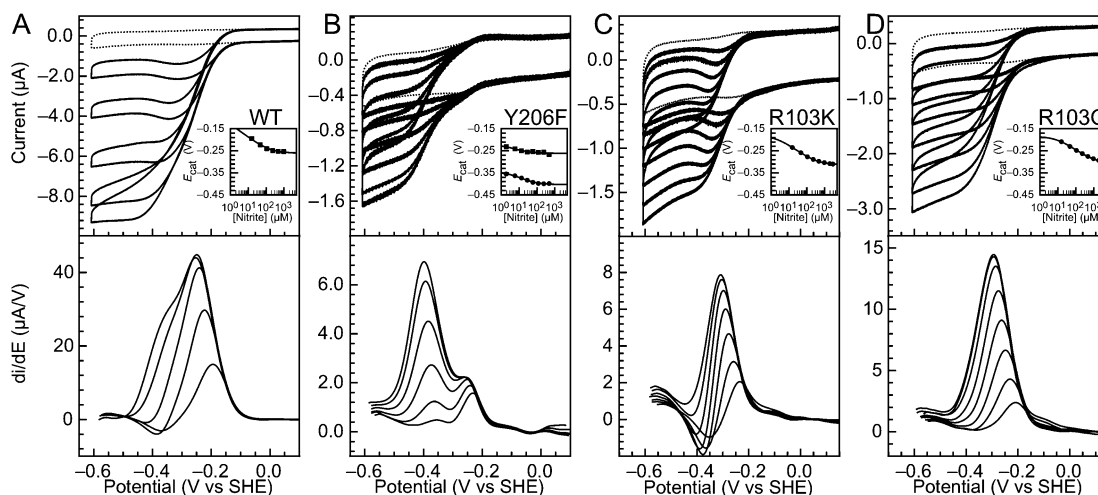
**Figure 2.** Current−potential profiles of (A) WT ccNiR and its (B) Y206F, (C) R103K, and (D) R103Q mutants. All experiments were performed at pH 7, 20 mV/s, and 20 °C, with an electrode rotation rate of 3000 rpm. Top panels show overlays of raw cyclic voltammograms recorded at increasing nitrite concentrations. Dotted cyclic voltammograms show data of ccNiR films recorded in the absence of nitrite. Bottom panels show first derivatives of baseline-subtracted reductive scans of the voltammograms. Insets show plots of $E_{cat}$ values vs nitrite concentration fit to eq 3. Substrate concentrations were 16−473 μM for WT, 2−120 μM for Y206F, 16 μM to 1.9 mM for R103K, and 76 μM to 8.4 mM for R103Q.
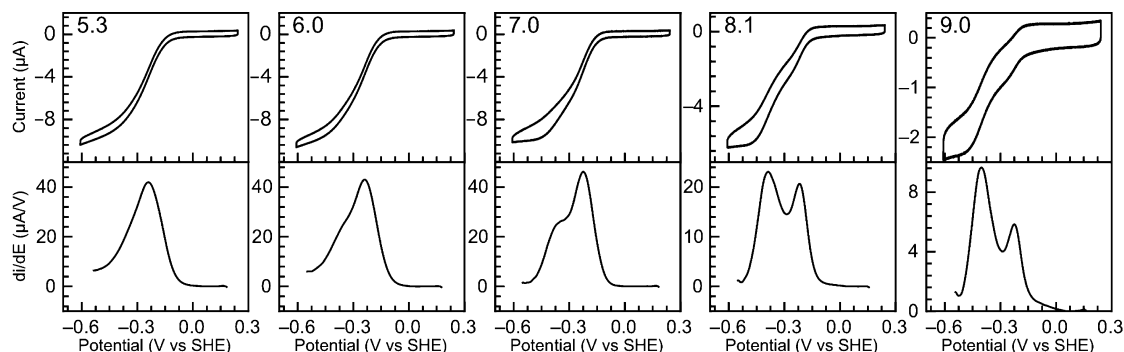


**Figure 3.** Dependence of the ccNiR catalytic waveform on pH. All scans were recorded at 500 μM nitrite, 20 mV/s, and 20 °C, with an electrode rotation rate of 3000 rpm. Top panels show raw voltammograms. Bottom panels show first derivatives of baseline-subtracted reductive scans. The cell solution pH is shown at the top left of each panel.

The positions of both catalytic features shift with increasing nitrite concentrations, with $E_{cat1}$ and $E_{cat2}$ spanning potential ranges of −230 to −270 mV and −355 to −400 mV, respectively (Figure 2B, inset).

Like those of wild-type ccNiR, the relative contributions of each of the catalytic features to the overall waveform vary with pH. In Y206F ccNiR, however, this dependence is distinct from that of WT (Figure 1 of the Supporting Information). The low-potential feature dominates the catalytic waveform across a wide pH range of 5−9, contrary to what is observed for the WT enzyme (Figure 3). Under the conditions tested, $E_{cat1}$ is barely detectable at most pH values. Only above pH 9, when the overall enzymatic activity of Y206F is very low, does the high-potential ($E_{cat1}$) feature appear to be approximately the same size as the low-potential feature.

**R103K Catalytic Current−Potential Profile.** The R103K variant also causes a distinct change in the catalytic current−potential profile (Figure 2C). Only a single catalytic feature is present across all concentrations of nitrite (i.e., there is no boost), yet distinct switch behavior (attenuation in activity at approximately −350 mV) is present at nitrite concentrations up to $K_M$ for R103K. Also, the position of the primarily catalytic feature shifts to more negative potentials as the concentration

of nitrite is increased and spans a range of −235 to −310 mV (Figure 2C, inset).

**R103Q Catalytic Current−Potential Profile.** Mutation of R103 to a glutamine residue also causes a significant change to the overall catalytic waveforms observed during turnover of ccNiR (Figure 2D). As seen for R103K, a single catalytic feature is observed across the entire range of nitrite concentrations tested, yet in contrast to R103K, at pH 7 no switch feature is observed nor is an attenuation of activity ever observed. As with WT ccNiR, the catalytic feature observed during R103Q ccNiR turnover becomes more negative with an increasing substrate concentration and covers a potential range of −210 to −300 mV (Figure 2D, inset), contained within the potential ranges of $E_{cat1}$ and $E_{cat2}$ observed during WT nitrite turnover.

**pH Dependence of WT ccNiR Nitrite Turnover.** Variable-pH experiments reveal that the position of the lower-potential catalytic feature associated with nitrite reduction, $E_{cat2}$, shifts with pH, while the position of the high-potential feature, $E_{cat1}$, is invariant with pH over a wide range of pH values (Figure 4A). The position of $E_{cat2}$ is pH-independent at pH values less than ∼6.5 and greater than ∼9. In the pH range of 6.5−9, the position of $E_{cat2}$ becomes more negative as the pH of the electrochemical cell solution is increased.
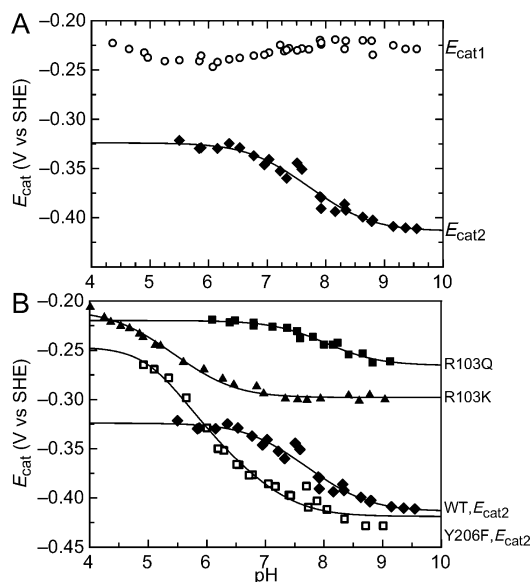
**Figure 4.** pH dependence of catalytic features during WT and mutant ccNiR nitrite turnover. (A) Plot of $E_{cat1}$ ($\bigcirc$) and $E_{cat2}$ ($\blacklozenge$) for WT ccNiR. (B) Plots of $E_{cat2}$ values for WT ($\blacklozenge$), Y206F ($\square$), R103Q ($\blacksquare$), and R103K ($\blacktriangle$). Experiments were conducted at 500 $\mu$M nitrite, 20 °C, and 20 mV/s, with an electrode rotation rate of 3000 rpm. $E_{cat2}$ data for WT, R103Q, and R103K are fit to eq 1, and $E_{cat2}$ data for Y206F are fit to eq 2.

Measuring the position of $E_{cat}$ values at the pH extremes is made difficult by the lower activity of ccNiR in these pH regions. Additionally, at more acidic pH values, measurement of the position of $E_{cat2}$ is further complicated because this feature overlaps significantly with $E_{cat1}$, making the two features difficult to resolve.

The pH dependence of $E_{cat2}$ for WT ccNiR can be readily fit to a model of proton-coupled electron transfer, in which a one-electron process is coupled to a single protonation event (eq 1)

$$E_{cat} = E_{acid} - 0.059 \times \log\left(\frac{10^{-pH} + 10^{-pK_{ox}}}{10^{-pH} + 10^{-pK_{red}}}\right) \quad (1)$$

where the fitted parameters are summarized in Table 2.

**Table 2. Fitted Parameters from Fitting of pH Dependence Data**

|  | $E_{acid}$ (mV) | $pK_{ox1}$ | $pK_{red1}$ | $pK_{ox2}$ | $pK_{red2}$ |
|---|---|---|---|---|---|
| WT | −324 | 7.0 | 8.5 | NA[b] | NA[b] |
| Y206F | −246 | 5.1 | 5.7 | 5.1 | 7.4 |
| R103Q | −220 | 7.6 | ≥8.4[a] | NA[b] | NA[b] |
| R103K | ≤−209 | ≤4.7 | 6.2 | NA[b] | NA[b] |

[a]This value is estimated because of the low activity at the alkaline limit.
[b]Not available.

**pH Dependence of Y206F ccNiR.** Like that of WT, the high-potential catalytic feature ($E_{cat}$) observed during Y206F electrocatalysis is invariant with pH across a wide range of pH values (Figure 2 of the Supporting Information). The pH profile of $E_{cat2}$ is distinct (Figure 4B) and is not well-described by eq 1 (Figure 2 of the Supporting Information). The pH dependence of $E_{cat2}$ is composed of two distinct regions. Between pH 6 and 8, the $E_{cat}$ value changes with pH with a slope of −59 mV/pH unit, consistent with a one-electron one-proton process. At pH values between 5 and 6, $E_{cat}$ shifts with a

slope of −118 mV/pH unit, consistent with a one-electron two-proton process. These data can be described by a model that accounts for an additional protonation event (eq 2):[31]

$$E_{cat} = E_{acid} - 0.059 \times \log\left\{\left[1 + \frac{10^{-pK_{ox1}}}{10^{-pH}}\right.\right.$$
$$\left. + \frac{10^{-pK_{ox2}} \times 10^{-pK_{ox1}}}{(10^{-pH})^2}\right] \bigg/ \left[1 + \frac{10^{-pK_{red1}}}{10^{-pH}}\right.$$
$$\left.\left. + \frac{10^{-pK_{red1}} \times 10^{-pK_{red2}}}{(10^{-pH})^2}\right]\right\} \quad (2)$$

Using this model, we assume $pK_{ox1} = pK_{ox2}$, because of the absence of an additional detectable one-electron one-proton region below pH 5. While it is possible that the two $pK_{ox}$ values may be slightly different from one another, this cannot be reliably determined from our data. On the basis of the results of the fit, the $pK_{red}$ and $pK_{ox}$ values associated with the −59 mV/pH unit region ($pK_{ox2}$ and $pK_{red2}$, respectively) are shifted toward the acidic direction compared to those of WT (Table 2).

**pH Dependence of R103Q ccNiR.** The pH dependence of the single catalytic feature observed during R103Q nitrite turnover is well-described by eq 1 (Figure 4B). Despite the one-electron one-proton stoichiometry for the observed PCET process, the pH dependence of R103Q is distinct from that of WT ccNiR. Most notably, the value of $E_{cat}$ at the acidic limit ($E_{acid}$) is shifted by approximately 100 mV relative to that of WT (Table 2). We found that this difference could not be accounted for by the larger $K_M$ exhibited by R103Q, because repeating the pH dependence experiment in the presence of approximately saturating (3 mM) nitrite decreases the difference in $E_{acid}$ between R103Q and WT to only approximately 90 mV (Figure 3 of the Supporting Information).

The $pK_{ox}$ values for R103Q are shifted in the alkaline direction by approximately half a pH unit (Table 2). It is not clear from these data where the pH invariant region at the alkaline limit begins because the low activity of R103Q ccNiR at pH >9 precludes measurement of an $E_{cat}$ value. Therefore, the reported $pK_a$ values are taken to be estimates.

**pH Dependence of R103K ccNiR.** While the pH dependence of the single catalytic feature observed during R103K electrocatalysis is well-described by eq 1, the data are distinct from those of WT, Y206F, and R103Q ccNiR, such that the $E_{cat}$ feature is invariant with pH between pH ~7 and 9 (Figure 4B). This corresponds to a shift in $pK_a$ values of nearly two pH units. A pH invariant acidic region could not be detected and can therefore only be estimated (Table 2). On the basis of our estimates, we have found that the $E_{acid}$ value for R103K has shifted to more positive potentials by at least 100 mV.

**Substrate Dependence of WT and Variant ccNiR $E_{cat}$ Values.** The positions of all detected catalytic features were dependent on the concentration of substrate (Figure 2, inset), and could be described by eq 3:[32]

$$E_{cat} = E_m([S] = 0) + \frac{2.3RT}{nF} \log\left(\frac{1 + [S]/K_{ox}^{NO_2^-}}{1 + [S]/K_{red}^{NO_2^-}}\right) \quad (3)$$

At pH 7, the $E_{cat2}$ feature is not well-defined for WT ccNiR (Figure 2). However, at pH 8.3, this feature is better separated

from $E_{cat1}$, and the substrate dependence of both features is apparent (Figure 4 of the Supporting Information).

**Production of Ammonia by WT and Variant ccNiR.** Quantification of moles of reducing equivalents consumed per mole of ammonia produced was performed on WT ccNiR and its variants. Within error, all variants produced the expected one ammonia for every six reducing equivalents consumed, strongly indicating that all tested ccNiR variants are competent in conducting the six-electron reduction of nitrite to ammonia, regardless of the overall $k_{cat}$ (Table 1).

## ■ DISCUSSION

PCET is a feature of numerous enzymes involved in a wide variety of different chemical processes and plays an especially important role in multielectron multiproton reactions. In this study, we have used PFV to directly probe proton coupling that occurs during the six-electron seven-proton reduction of nitrite to ammonia and show that PFV can describe multiple contributions to catalysis, some of which are proton-dependent while others are not.

Cytochrome $c$ nitrite reductase has been a model for understanding multielectron multiproton catalysis for more than a decade.[16] However, until now, few details of the roles of individual amino acid residues within the active site or how proton-coupled steps that occur during the rate-limiting step of ccNiR catalysis are controlled have been presented. This work offers a first look at the roles of the individual active site amino acids in governing activity, electrochemical properties, proton-coupled redox steps, and competence to conduct the full reduction of nitrite to ammonia. Importantly, we have found that while individual amino acids are responsible for tuning the properties of the active site, no single amino acid is responsible for gating proton delivery and allowing the enzyme to conduct the full reduction of nitrite to ammonia.

**Active Site Mutations Alter Rate-Limiting Steps of Catalysis in ccNiR.** To date, all ccNiRs studied by protein film voltammetry exhibit a similar current–potential profile, characterized by attenuations and boosts in activity that depend on the concentration of substrate present and the applied potential.[24,26] The physical basis of either phase of electrocatalysis is still not well-defined, although the relative dominance of one component of current likely represents a shift in the rate-limiting steps of catalysis, in a fashion that depends upon the applied potential.[33] One inference drawn from this model historically is that $E_{cat2}$ may be due to a secondary redox process that accelerates the rate of catalysis, such as an alternative relay to the active site heme.[34,35] However, the substrate dependence of both $E_{cat1}$ and $E_{cat2}$ strongly suggests that these features are the result of processes occurring at the active site (Figure 2 and Figure 4 of the Supporting Information) and suggest redox steps occurring during the conversion of nitrite to ammonia. We therefore interpret $E_{cat1}$ and $E_{cat2}$ as indicating rate-limiting steps of catalysis that involve chemistry occurring at the active site.

Using site-directed mutagenesis, we can alter the appearance of the phases that comprise a catalytic wave (Figure 2). The Y206F, R103Q, and R103K variants all exhibit current–potential profiles significantly altered compared to that of the wild-type enzyme under the same conditions. Given that all of these mutations are at the active site of ccNiR, the altered profiles provide further evidence that the detected electron transfer steps are occurring at the active site.

Like WT ccNiR, the Y206F variant displays multiple phases within its catalytic signals; however, these phases are altered. In terms of potential, the $E_{cat1}$ and $E_{cat2}$ features for Y206F are far more distinct from one another at pH 7 than those of WT, which we interpret to be the result of the altered proton coupling (see below).

Surprisingly, changing R103 to a glutamine or a lysine has different effects on the current–potential profile of ccNiR, differentially altering the detected phases of catalysis (Figure 2). In the case of both variants, the current–potential profile consists of a single catalytic feature, contrary to that of WT ccNiR. R103K still exhibits the switch behavior, but in R103Q, only a single feature is observed. The position of this feature lies between $E_{cat1}$ and $E_{cat2}$ potentials observed in WT ccNiR.

Importantly, neither R103Q nor Y206F exhibits the switch behavior, while R103K does (at concentrations of nitrite up to the $K_M$). The switch feature has been hypothesized to be the result of uncompensated negative charge at the bis-His-ligated hemes that has been supported by the apparent increase in the prominence of the switch with increased pH, because at higher pH values there are fewer protons present to counteract this buildup of negative charge.[27] However, the modulation of the presence of the switch by altering active site residues suggests the process responsible for the switch behavior occurs at or near the active site, rather than at hemes distant from the active site that are involved in relaying ET reactions solely.

**Catalysis Is Governed by One-Electron Events and One-Electron One-Proton events.** Previous electrocatalytic analysis of *S. oneidensis* ccNiR indicated that the nature of the rate-determining step for nitrite reduction at pH 8.3 varied with applied potential and likely involved the transfer of a single electron.[24] Our current data add to these findings by confirming that at least one ET event (i.e., $E_{cat2}$) has one-electron one-proton stoichiometry, and all detected ET events are consistent with $n = 1$ processes (Table 2 of the Supporting Information). The presence of a proton-coupled redox event during nitrite catalysis is clearly demonstrated by the pH dependence of the $E_{cat2}$ feature at saturating nitrite concentrations, which fits well to a one-electron one-proton model (Figure 4).

Our findings also reveal that during the onset of catalysis, the rate of the conversion of nitrite to ammonia is governed by an electron transfer event that is not proton-coupled ($E_{cat1}$). This suggests that within the catalytic mechanism, both proton-coupled redox steps and an ET step that is not coupled to a protonation exist. The presence of both proton-coupled ($E_{cat2}$) and proton-independent ($E_{cat1}$) electron transfer events suggests that within the ccNiR catalytic mechanism, not all ET steps necessitate a coupled proton transfer.

**Active Site Residues Impact Proton-Coupled Redox Chemistry during Electrocatalysis.** Our data largely confirm the hypothesized involvement of the His257, Arg103, and Tyr206 residues in proton-coupled redox chemistry, as described by recent computational studies.[16,21,22,25] For example, computational evidence suggests Tyr206 acts as a proton donor during catalysis, possibly during the final step in the six-electron reduction (Scheme 1),[25] and Tyr206 has been shown to be important for the activity of *Wolinella* ccNiR.[36] Here, the altered proton dependence of Y206F confirms that this residue does play a role in PCET during conversion of nitrite to ammonia (Figure 4B). First, the similarity between the current–potential profiles for Y206F and WT where $E_{cat1}$ is pH-independent and $E_{cat2}$ is pH-dependent strongly suggests

that the same processes are observed in each case. The pH dependence profile for the Y206F variant consists of two regions, an alkaline region and an acidic region. The alkaline region of pH dependence has a slope consistent with a one-electron one-proton process with $pK_a$ values shifted in the acidic direction relative to those of WT ccNiR. The pH dependence region between pH 6 and 8 has a slope of approximately −59 mV/pH, which is consistent with a one-proton one-electron process. We interpret this pH-dependent region to be the same process that is observed during WT turnover for $E_{cat2}$, although the $pK_a$ values are apparently altered by the absence of the terminal hydroxyl group of the tyrosine residue. The pH dependence region from pH 5 to 6 appears to be a proton-coupled redox process that in WT is outside the physiological pH range; the Y206F mutation apparently alters the $pK_a$ values of this process such that they are now accessible at higher pH values. Together, we interpret these data to indicate that Y206 is involved in tuning the $pK_a$ values of the proton-coupled redox event observed in PFV. Altering this residue alters the $pK_a$ values of the observed proton-coupled redox process and therefore alters the pH dependence profile of ccNiR.

Mutation of Arg103 to Gln or Lys also alters the pH dependence profile of ccNiR (Figure 4B). The R103Q mutation causes the $pK_a$ values associated with the proton-coupled redox event to shift slightly in the alkaline direction, although importantly, the stoichiometry of the proton-coupled process is not altered compared to that of WT. In the case of the R103K variant, the $pK_a$ values shift in the acidic direction, where the catalytic feature is no longer proton-coupled at physiological pH. These data support the hypothesis that R103 plays a role in tuning the $pK_a$ values of the detected proton-coupled redox step.

Rationalizing how the Y206F, R103K, and R103Q variants differentially affect the properties of ccNiR catalysis can be assisted by examination of the high-resolution crystal structure of the ccNiR from *W. succinnogenes*, which reveals a number of waters within the active site (Figure 1B). Together with R103, H257, and Y206, these waters make up an extensive hydrogen bonding network within the active site. We hypothesize that even if crystallographically resolved waters were the specific proton donors to intermediate species produced during catalysis, Y206 and R103 are able to influence this step through the hydrogen bonding network.

**R103 Contributes to Substrate Binding and Modulates the Operating Potential of Catalysis.** Our finding that R103Q has a significantly altered $K_M$ suggests that the residue plays at least a partial role in stabilizing binding of substrate, likely through a charge−charge interaction between negatively charged substrate and the positively charged guanidinium group. This partial effect is confirmed by variant R103K, which has a $K_M$ value that is closer to that of WT. More significantly, the entire pH profiles for the R103 variants are shifted by nearly 100 mV in the positive direction, suggesting that R103 plays a direct role in tuning the potential of this proton-coupled redox step, likely by directly influencing the potential of the active site heme. Inspection of the crystal structures of all ccNiRs indicates that the arginine nitrogen forms a hydrogen bonding contact with a heme propionate (C7) (Figure 1B). Previous studies have shown that the protonation state of heme propionates, which can be influenced by the presence of nearby residues, can play a large role in determining the potential of a heme.[37,38] The interaction

between R103 and the active site heme propionate is apparently altered in both the R103Q and R103K variants, potentially altering the protonation state of the heme propionate, providing an explanation for the difference in the operating potential of R103Q and -K variants compared to that of WT ccNiR. However, this apparent change in the potential of the active site heme could not be detected using protein film voltammetry, and all variants tested here have similar electrochemical responses (Figure 5 of the Supporting Information). Our inability to observe the altered potential of the active site heme is likely due to the highly overlapping nature of signals from the hemes in ccNiR.

**Ability of ccNiR Active Site Variants To Catalyze Six-Electron Reduction of Nitrite to Ammonia.** Despite the apparent differences in steady-state kinetic values, electrocatalytic profiles, and $pK_a$ values of PCET, all variants retain the ability to conduct the full reduction of nitrite to ammonia in the expected six electron equivalents consumed per one ammonia produced (Table 1). As it is easy to imagine that a diminished degree of proton delivery may result in the release of partially reduced products, such a finding is truly surprising, as all residues considered here have been implicated in required proton delivery, through computational analyses. For example, it has been suggested that H257 participates in the first N−O bond cleavage during nitrite catalysis by acting as a proton donor. Additionally, previous work on the *Desulfovibrio desulfuricans* enzyme using electrochemistry suggested an active site histidine is a potential proton donor to the heme−substrate complex during catalysis,[28,39] yet our results clearly demonstrate that when H257 cannot act as a proton donor, the complete reaction still proceeds, although at a reduced rate. The proton likely instead comes from waters within the active site, or alternatively Arg103, as has been proposed previously, although this must occur at a much slower rate.[25]

Similarly, according to DFT studies, residues Y206 and R103 also likely act as proton donors during the reduction of nitrite to ammonia.[25] Although alteration of Y206 and R103 residues reduces activity, they do so to a lesser extent than H257. R103 apparently has additional roles, which are charge stabilization of the negatively charged nitrite as well as possibly tuning of the active site heme potential.

These results suggest that no individual residue tested here is essential for directing or gating the complete catalytic reduction of nitrite to ammonia; rather, the residues act collectively to accelerate the completed reaction, which is feasible here as electrons are never limiting.

## ■ CONCLUSIONS

The data presented here offer insight into how multiple electron transfer and protonation events are controlled within the ccNiR active site during catalytic reduction of nitrite. First, our data clearly demonstrate that ccNiR catalysis is governed by two distinct phases: a one-electron one-proton event and a one-electron event not coupled to a proton transfer. Second, the ability of the ccNiR variants tested here to conduct their full reaction, with reduced rates and altered $pK_a$ values, demonstrates the importance of the precise control of proton-coupled electron transfer steps that is required to achieve high turnover numbers at physiological pH values. This control is likely mediated though an extensive hydrogen bonding network, involving both the protein and solvent waters. Future studies should focus on what factors drive the

direction of catalysis, as well as what roles each individual residue plays at each ET step throughout the catalytic cycle.

## ■ ASSOCIATED CONTENT

### ⓢ Supporting Information

Primers used for construction of ccNiR variants, table of half-height widths from first derivatives of catalytic waves, dependence of wave shape and positions of features on pH for the Y206F variant, pH dependence of the R103Q variant at 3 mM nitrite, dependence of WT ccNiR $E_{cat}$ values on nitrite concentration, and nonturnover electrochemical signals for WT ccNiR and its variants. This material is available free of charge via the Internet at http://pubs.acs.org.

## ■ AUTHOR INFORMATION

### Corresponding Author

*Department of Chemistry, Boston University, 590 Commonwealth Ave., Boston, MA 02215. E-mail: Elliott@bu.edu. Telephone: (617) 358-2816. Fax: (617) 353-6466.

### Notes

The authors declare no competing financial interest.

## ■ ACKNOWLEDGMENTS

## ■ ABBREVIATIONS

ccNiR, cytochrome *c* nitrite reductase; PFV, protein film voltammetry; PCET, proton-coupled electron transfer; PMSF, phenylmethanesulfonyl fluoride; DTT, dithiothreitol; TEV, tobacco etch virus protease; DFT, density functional theory; ET, electron transfer.

## ■ REFERENCES

(1) Crane, B. R., Siegel, L. M., and Getzoff, E. D. (1997) Probing the catalytic mechanism of sulfite reductase by X-ray crystallography: Structures of the *Escherichia coli* hemoprotein in complex with substrates, inhibitors, intermediates, and products. *Biochemistry 36*, 12120−12137.

(2) Gagliardi, C. J., Westlake, B. C., Kent, C. A., Paul, J. J., Papanikolas, J. M., and Meyer, T. J. (2010) Integrating proton coupled electron transfer (PCET) and excited states. *Coord. Chem. Rev. 254*, 2459−2471.

(3) Weinberg, D. R., Gagliardi, C. J., Hull, J. F., Murphy, C. F., Kent, C. A., Westlake, B. C., Paul, A., Ess, D. H., McCafferty, D. G., and Meyer, T. J. (2012) Proton-coupled electron transfer. *Chem. Rev. 112*, 4016−4093.

(4) Reece, S. Y., and Nocera, D. G. (2009) Proton-coupled electron transfer in biology: Results from synergistic studies in natural and model systems. *Annu. Rev. Biochem. 78*, 673−699.

(5) Hammarstrom, L., and Styring, S. (2008) Coupled electron transfers in artificial photosynthesis. *Philos. Trans. R. Soc., B 363*, 1283−1291.

(6) Huynh, M. H., and Meyer, T. J. (2007) Proton-coupled electron transfer. *Chem. Rev. 107*, 5004−5064.

(7) Stubbe, J., Nocera, D. G., Yee, C. S., and Chang, M. C. (2003) Radical initiation in the class I ribonucleotide reductase: Long-range proton-coupled electron transfer? *Chem. Rev. 103*, 2167−2202.

(8) Reece, S. Y., Hodgkiss, J. M., Stubbe, J., and Nocera, D. G. (2006) Proton-coupled electron transfer: The mechanistic underpinning for radical transport and catalysis in biology. *Philos. Trans. R. Soc., B 361*, 1351−1364.

(9) Chang, C. J., Chang, M. C., Damrauer, N. H., and Nocera, D. G. (2004) Proton-coupled electron transfer: A unifying mechanism for biological charge transport, amino acid radical initiation and propagation, and bond making/breaking reactions of water and oxygen. *Biochim. Biophys. Acta 1655*, 13−28.

(10) Cukier, R. I. (2004) Theory and simulation of proton-coupled electron transfer, hydrogen-atom transfer, and proton translocation in proteins. *Biochim. Biophys. Acta 1655*, 37−44.

(11) Umena, Y., Kawakami, K., Shen, J. R., and Kamiya, N. (2011) Crystal structure of oxygen-evolving photosystem II at a resolution of 1.9 Å. *Nature 473*, 55−60.

(12) Meyer, T. J., Huynh, M. H., and Thorp, H. H. (2007) The possible role of proton-coupled electron transfer (PCET) in water oxidation by photosystem II. *Angew. Chem., Int. Ed. 46*, 5284−5304.

(13) Belevich, I., Verkhovsky, M. I., and Wikstrom, M. (2006) Proton-coupled electron transfer drives the proton pump of cytochrome c oxidase. *Nature 440*, 829−832.

(14) Kaila, V. R. I., Verkhovsky, M. I., and Wikstrom, M. (2010) Proton-Coupled Electron Transfer in Cytochrome Oxidase. *Chem. Rev. 110*, 7062−7081.

(15) Simon, J. (2002) Enzymology and bioenergetics of respiratory nitrite ammonification. *FEMS Microbiol. Rev. 26*, 285−309.

(16) Einsle, O., Messerschmidt, A., Huber, R., Kroneck, P. M., and Neese, F. (2002) Mechanism of the six-electron reduction of nitrite to ammonia by cytochrome c nitrite reductase. *J. Am. Chem. Soc. 124*, 11737−11745.

(17) Stach, P., Einsle, O., Schumacher, W., Kurun, E., and Kroneck, P. M. (2000) Bacterial cytochrome c nitrite reductase: New structural and functional aspects. *J. Inorg. Biochem. 79*, 381−385.

(18) Kajie, S., and Anraku, Y. (1986) Purification of a hexaheme cytochrome $c_{552}$ from *Escherichia coli* K 12 and its properties as a nitrite reductase. *Eur. J. Biochem. 154*, 457−463.

(19) Youngblut, M., Judd, E. T., Srajer, V., Sayyed, B., Goelzer, T., Elliott, S. J., Schmidt, M., and Pacheco, A. A. (2012) Laue crystal structure of *Shewanella oneidensis* cytochrome c nitrite reductase from a high-yield expression system. *JBIC, J. Biol. Inorg. Chem. 17*, 647−662.

(20) Bamford, V. A., Angove, H. C., Seward, H. E., Thomson, A. J., Cole, J. A., Butt, J. N., Hemmings, A. M., and Richardson, D. J. (2002) Structure and spectroscopy of the periplasmic cytochrome c nitrite reductase from *Escherichia coli*. *Biochemistry 41*, 2921−2931.

(21) Bykov, D., and Neese, F. (2012) Reductive activation of the heme iron-nitrosyl intermediate in the reaction mechanism of cytochrome c nitrite reductase: A theoretical study. *JBIC, J. Biol. Inorg. Chem. 17*, 741−760.

(22) Bykov, D., and Neese, F. (2011) Substrate binding and activation in the active site of cytochrome c nitrite reductase: A density functional study. *JBIC, J. Biol. Inorg. Chem. 16*, 417−430.

(23) Bykov, D., Plog, M., and Neese, F. (2014) Heme-bound nitroxyl, hydroxylamine, and ammonia ligands as intermediates in the reaction cycle of cytochrome c nitrite reductase: A theoretical study. *JBIC, J. Biol. Inorg. Chem. 19*, 97−112.

(24) Judd, E. T., Youngblut, M., Pacheco, A. A., and Elliott, S. J. (2012) Direct electrochemistry of *Shewanella oneidensis* cytochrome c nitrite reductase: Evidence of interactions across the dimeric interface. *Biochemistry 51*, 10175−10185.

(25) Bykov, D., Plog, M., and Neese, F. (2014) Heme-bound nitroxyl, hydroxylamine, and ammonia ligands as intermediates in the reaction cycle of cytochrome c nitrite reductase: A theoretical study. *JBIC, J. Biol. Inorg. Chem. 19*, 97−112.

(26) Angove, H. C., Cole, J. A., Richardson, D. J., and Butt, J. N. (2002) Protein film voltammetry reveals distinctive fingerprints of nitrite and hydroxylamine reduction by a cytochrome c nitrite reductase. *J. Biol. Chem. 277*, 23374−23381.

(27) Gwyer, J. D., Richardson, D. J., and Butt, J. N. (2005) Diode or tunnel-diode characteristics? Resolving the catalytic consequences of proton coupled electron transfer in a multi-centered oxidoreductase. *J. Am. Chem. Soc. 127*, 14964−14965.

(28) Almeida, M. G., Silveira, C. M., Guigliarelli, B., Bertrand, P., Moura, J. J., Moura, I., and Leger, C. (2007) A needle in a haystack: The active site of the membrane-bound complex cytochrome c nitrite reductase. *FEBS Lett. 581*, 284−288.

(29) Chaney, A. L., and Marbach, E. P. (1962) Modified reagents for determination of urea and ammonia. *Clin. Chem. 8*, 130−132.

(30) Weatherburn, M. (1967) Phenol-hypochlorite reaction for determination of ammonia. *Anal. Chem. 39*, 971−974.

(31) Zu, Y., Fee, J. A., and Hirst, J. (2001) Complete thermodynamic characterization of reduction and protonation of the $bc_1$-type Rieske [2Fe-2S] center of *Thermus thermophilus. J. Am. Chem. Soc. 123*, 9906−9907.

(32) Léger, C., Heffron, K., Pershad, H. R., Maklashina, E., Luna-Chavez, C., Cecchini, G., Ackrell, B. A., and Armstrong, F. A. (2001) Enzyme electrokinetics: Energetics of succinate oxidation by fumarate reductase and succinate dehydrogenase. *Biochemistry 40*, 11234−11245.

(33) Léger, C., and Bertrand, P. (2008) Direct electrochemistry of redox enzymes as a tool for mechanistic studies. *Chem. Rev. 108*, 2379−2438.

(34) Heering, H. A., Weiner, J. H., and Armstrong, F. A. (1997) Direct Detection and Measurement of Electron Relays in a Multicentered Enzyme: Voltammetry of Electrode-Surface Films of *E. coli* Fumarate Reductase, an Iron-Sulfur Flavoprotein. *J. Am. Chem. Soc. 119*, 11628−11638.

(35) Heering, H. A., Hirst, J., and Armstrong, F. A. (1998) Interpreting the catalytic voltammetry of electroactive enzymes adsorbed on electrodes. *J. Phys. Chem. B 102*, 6889−6902.

(36) Lukat, P., Rudolf, M., Stach, P., Messerschmidt, A., Kroneck, P. M., Simon, J., and Einsle, O. (2008) Binding and reduction of sulfite by cytochrome c nitrite reductase. *Biochemistry 47*, 2080−2086.

(37) Voigt, P., and Knapp, E.-W. (2003) Tuning heme redox potentials in the cytochrome c subunit of photosynthetic reaction centers. *J. Biol. Chem. 278*, 51993−52001.

(38) Mao, J., Hauser, K., and Gunner, M. (2003) How cytochromes with different folds control heme redox potentials. *Biochemistry 42*, 9829−9840.

(39) Maia, L. B., and Moura, J. J. (2014) How biology handles nitrite. *Chem. Rev. 114*, 5273−5357.

(40) Einsle, O., Stach, P., Messerschmidt, A., Simon, J., Kroger, A., Huber, R., and Kroneck, P. M. (2000) Cytochrome c nitrite reductase from *Wolinella succinogenes*. Structure at 1.6 Å resolution, inhibitor binding, and heme-packing motifs. *J. Biol. Chem. 275*, 39608−39616.